Numerical simulation of reinforced concrete structures under impact loading

Živaljić, Nikolina; Nikolić, Željana; Smoljanović, Hrvoje; Munjiza, Ante

Source / Izvornik: **Materialwissenschaft und Werkstofftechnik, 2019, 50, 599 - 610**

Journal article, Published version
Rad u časopisu, Objavljena verzija rada (izdavačev PDF)

https://doi.org/10.1002/mawe.201800181

Permanent link / Trajna poveznica: https://urn.nsk.hr/urn:nbn:hr:123:637560

Numerical simulation of reinforced concrete structures under impact loading

Numerische Simulation des Verhaltens von Stahlbetonkonstruktionen unter Stoßbelastung

N. Živaljić[1], Ž. Nikolić[1], H. Smoljanović[1], A. Munjiza[1]

This study presents the performance of a combined finite-discrete element method for prediction of the structural response of reinforced concrete beams under impact loading. A combination of finite and discrete element methods enables the modelling of the concrete and the reinforcement before the concrete cracking, as well as a discontinuous nature of the concrete caused by fracture and fragmentation under high impact loading. Discretization of the concrete with triangular finite elements is coupled with one-dimensional reinforcing bars embedded inside the concrete finite elements. The cracking in the concrete activates the joint elements used to simulate the non-linear behavior of both concrete and reinforcement. Numerical analysis based on experimental test data has been carried out to simulate the main features of the reinforced concrete beams impacted by free-falling drop-weights. A high level of accuracy was demonstrated in various comparisons between the experimental tests and the analysis results, including peak displacement, crack pattern, damage level and failure modes of reinforced concrete beams.

Keywords: Crack pattern **/** finite-discrete element method **/** impact loading **/** numerical simulation **/** reinforced concrete beam

Diese Studie zeigt die Leistung der kombinierten Methode der Finite-Diskrete-Elemente zur Vorhersage der Reaktion in der Struktur von Stahlbetonträgern bei Stoßbelastung. Eine Kombination der Methoden der finiten und diskreten Elemente ermöglicht die Modellierung und die Bewehrung des Betons bevor dieser Risse aufweist sowie eine diskontinuierliche Beschaffenheit des Betons, verursacht durch Bruch und Zersplitterung unter hoher Stoßbelastung. Die Diskretisierung des Betons mit dreieckigen finiten Elementen ist mit eindimensionalen Bewehrungsstäben verbunden, die in die finiten Elemente des Betons eingebettet sind. Die Rissbildung im Beton aktiviert die Verbindungselemente, die eingesetzt werden um das nichtlineare Verhalten von Beton und Bewehrung zu simulieren. Es wurde eine numerische Analyse aufgrund experimenteller Testdaten durchgeführt, um die Hauptmerkmale der Stahlbetonträger zu simulieren, beeinflusst durch frei fallende Gewichte. Es wurde eine hohe Genauigkeit bei verschiedenen Vergleichen zwischen den experimentellen Tests und den Analyseergebnissen festgestellt, einschließlich Spitzenverschiebung, Rissmuster, Schadensgrad und Fehlerarten bei Stahlbetonträgern.

[1] Faculty of Civil Engineering, Architecture and Geodesy, University of Split, Matice Hrvatske 15, 21312 SPLIT, REPUBLIC OF CROATIA

Corresponding author: N. Živaljić, Faculty of Civil Engineering, Architecture and Geodesy, University of Split, Matice Hrvatske 15, 21312 SPLIT, REPUBLIC OF CROATIA,
E-Mail: nikolina.zivaljic@gradst.hr

Schlüsselwörter: Rissmuster / Methode der Finiten-Diskreten Elemente / Stoßbelastung / numerische Simulation / Stahlbetonträger

1 Introduction

The design of reinforced concrete structures resistant to the impact loading has been recognised as crucial in preventing the progressive collapse of these structures and protecting human life, especially in the last few decades, after frequent terrorist attacks around the world. Numerous studies have been conducted to date towards understanding and developing methodologies predicting the behaviour of these structures. However, it is difficult to name one commonly accepted method. The choice of the method depends on the type, geometry or required information about the structural behaviour. In order to determine the local response of the members independent of its global response, one can use empirical formulae [1, 2]. Analytical approaches using mass-spring systems are used in order to determine global deformations [3–6]. As a consequence of neglecting the local effects, this approach may yield inaccurate results. The majority of the research in global response was carried out on reinforced concrete beams, since the local damage becomes considerably more important in the case of thin slabs under impacts. Over the past few decades, several studies have been reported for reinforced concrete members subjected to impact loading [7–13]. Numerical methods, such as the finite element method, are the most used tools in the analysis of impact behaviour of reinforced concrete members, taking into account their global and local response.

The finite element packages which are used for impact analysis of reinforced concrete structures require sophisticated numerical models of material behaviour and contact interaction [14–23].

The fragmentation that may occur after the impact loading could not be considered by using the finite element method. Therefore, alternative methods were developed considering the discontinuities in the medium, such as the discrete element method [24–27].

It is important to notice that any comprehensive failure simulation needs to address the elastic and elasto-plastic behaviour of the structural components including failure, fracture, fragmentation, transient motion, contact impact, collapse, energy dissipation mechanisms and the state of rest. To this end, a recently developed state of the art in finite-discrete element method offers a capability to address all of these phenomena.

The finite-discrete element method was primarily developed mainly for the simulation of fracturing problems considering deformable particles that may split and separate during the analysis [28]. Up to date the finite-discrete element method found its application in analysis of many types of structures such as reinforced concrete structures, beam type structures, shell structures etc. [29–33]. The main processes included in the finite-discrete element method are contact detection, contact interaction, finite strain elasticity, as well as fracture and fragmentation. A contact detection algorithm has to detect couples of discrete elements close to each other and eliminate couples which are too far and cannot possibly be in contact [34]. The interaction between discrete elements is considered through the contact interaction algorithm based on potential contact forces [35] including the Coulomb-type law for friction. The method uses an explicit numerical integration of the equation of motion.

In order to analyse and predict the collapse of the reinforced concrete structures under dynamic loading, finite-discrete element method is extended with a new numerical model of the reinforcing bar [30, 31]. The concrete structure is discretised by constant strain triangular finite elements, whereas the reinforcing bars are modelled with the linear one-dimensional elements implemented inside the concrete finite elements. Material non-linearity, including the cracking of the concrete, plastic deformation of the steel, as well as the cyclic behaviour of both materials during dynamic loading are considered through the concrete and steel joint elements which are implemented within a finite element mesh.

In this paper, the combined finite discrete model for reinforced concrete structures subjected to dynamic loading was extended in order to simulate the behaviour of these structures under impact loading [30, 31]. Some of the most important effects of the

model are the increases in dynamic tensile strength under high impact loading, reliable representation of the cracks, interaction between the reinforcement and the concrete considering the steel strain-slip relation, the influence of adjacent cracks on the slip of the reinforcing bar, local slip of the reinforcing bar near the crack plane when the bar undergoes high plastic deformation and the influence of the curvature of the reinforcing bar to yield stress reduction of the steel.

The results of the performed numerical analyses were compared to the experimental tests of reinforced concrete beams impacted by free-falling drop-weights [36].

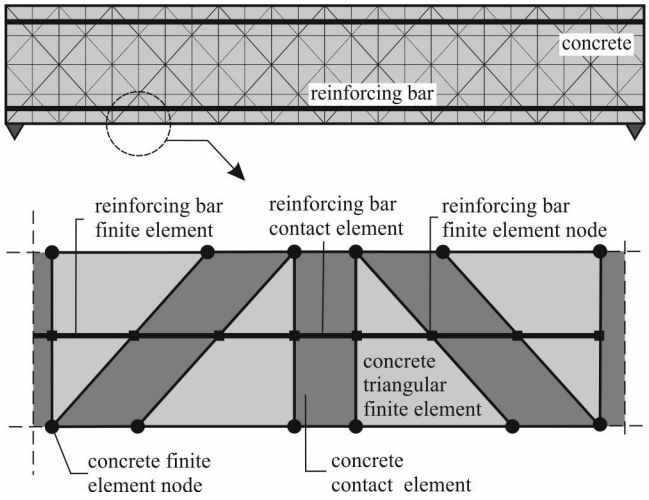

Figure 1. Discretisation of reinforced concrete structure.
Bild 1. Diskretisierung der Stahlbetonstruktur.

2 The modelling approach

2.1 Discretisation of the reinforced concrete structure

The presented model, developed for the plane reinforced concrete structures, uses discretisation by constant strain triangular finite elements for the concrete and one-dimensional elements for the reinforcing bars. Reinforcing bar finite elements are placed inside the concrete finite elements [30, 31]. The material non-linearity, fracture and fragmentation are considered through the joint elements which are implemented within the finite element mesh. The interaction between discrete elements is modelled through the contact interaction algorithm based on the principle of potential contact forces and the Coulomb-type law for friction [34, 37]. The method uses an explicit numerical integration of the equation of motion.

The model of the reinforced concrete structure with an embedded reinforcing bar is presented, *Figure 1*. The reinforcing bar was defined by its initial and end points. The intersection between the sides of triangular concrete finite elements and reinforcing bars provides the reinforcing finite elements and reinforcing joint elements, Figure 1.

In this model, the structure behaves as a continuum until the opening of the crack. It is assumed that the whole nonlinearity produced in a localisation zone on a surface of discontinuity of the displacement field is simulated inside the joint element. The initiation of a crack in the concrete leads to the deformation in the reinforcing bar joint element [30, 31]. In the presented model, the bond deterioration between the concrete and the reinforcing bar was taken into account in the reinforcing bar joint element, which means that the strain of the reinforcing bar finite element is determined from the strain of the parent triangular finite element. Taking into account the linear-elastic relationship between stress and strain in the reinforcing bar finite element and cross-sectional area of the reinforcing bar, the forces acting in the reinforcing bar finite element nodes can be obtained. These forces are distributed into the nodes of the parent concrete triangular element in the form of equivalent nodal forces [30, 31].

2.2 Contact interaction and deformability of discrete elements

The combined finite-discrete element method is aimed at problems involving transient dynamics of systems comprising large number of deformable bodies which are represented by a single discrete element that interacts with adjacent discrete elements [28]. Each discrete element has its own finite element mesh which is used to analyse the deformability, fracture and fragmentation. The main processes included in the finite-discrete element method are contact detection, contact interaction, finite strain elasticity as well as fracture and fragmentation.

A contact detection algorithm has to detect the couples of adjacent discrete elements and eliminate the couples which are too far apart and cannot be in contact [34]. The total process time of this algorithm required to detect all contacting couples is indeed proportional to the total number of discrete elements.

The contact interaction between the discrete elements produces the distributed normal and frictional interaction forces which are computed by using the penalty function method [35]. The procedure is based on the assumption that small penetrations of contacting elements generate distributed normal contact forces depending on the size and shape of the overlapping area and stiffness parameter referred to as normal penalty coefficient p_n. The calculated contact force $\mathbf{f}_n$ is distributed around the nodes surrounding the contact in order to preserve the system from artificial stress concentration. In the tangential direction, the frictional interaction forces $\mathbf{f}_t$ are calculated by using the tangential penalty coefficient p_t and the tangential displacement vector $\boldsymbol{\delta}_t$ between the elements. If $\mathbf{f}_t$ is greater than the friction force satisfying the Coulomb friction law $|\mathbf{f}_t| > \mu|\mathbf{f}_n|$, the particles slide over each other, and the tangential force is calculated by using the total normal contact force $\mathbf{f}_t = -\mu\ \mathbf{f}_n$, where μ is the sliding friction coefficient.

The stress and strain relation, in constant strain triangular finite element, is implemented by using the Hooke's law according to:

$$T = \frac{E}{1+v}\check{\mathrm{E}}_{\mathrm{d}} + \frac{E}{1+2v}\check{\mathrm{E}}_{\mathrm{s}} + \bar{\mu}\boldsymbol{D} \tag{1}$$

where $\mathbf{T}$ is the Cauchy stress tensor, E is the modulus of elasticity, v is Poisson's ratio, $\check{\boldsymbol{E}}_{\boldsymbol{d}}$ is the shape changing part and $\check{\boldsymbol{E}}_{\boldsymbol{s}}$ is the volume changing part of Green-St. Venant's strain tensor, $\bar{\mu}$ is the damping coefficient and $\mathbf{D}$ is the rate of the deformation tensor [28].

2.3 Concrete material model

The non-linear behaviour of the concrete is modelled by the joint elements which are designed for the simulation of the crack initiation and propagation in tension and shear [30, 38]. In this model, it is assumed that the crack walls coincide with the finite element edges. It is achieved in a way that every single discrete element is associated with its separate finite element mesh. Hence, initially, the total number of nodes for each of the finite element meshes is doubled and the nodes are held together through the penalty function method.

The separation of these edges induces the bonding stress which is taken to be the function of the size of separation δ, *Figure 2*. The area under stress-displacement curve represents the energy release rate $G_f = 2\gamma$, where γ is the surface energy, i. e. the energy needed to extend the crack surface by a unit area.

Before reaching the tensile strength f_t, there is no separation of the element edges which is enforced through the penalty function method [38]. For the separation $\delta \leq \delta_t$, the bonding stress is provided by:

$$\sigma_{cj} = \left[\frac{2\delta}{\delta_t} - \left(\frac{\delta}{\delta_t}\right)^2\right] f_t \tag{2}$$

where $\delta_t = 2hf/p_n$ is the separation corresponding to the bonding stress equal to the tensile strength f_t, h is the size of the particular element and p_n is normal penalty coefficient.

After reaching the tensile strength f_t, the stress decreases with an increasing separation δ, and, at $\delta = \delta_c$, the bonding stress tends to zero. For the sep-

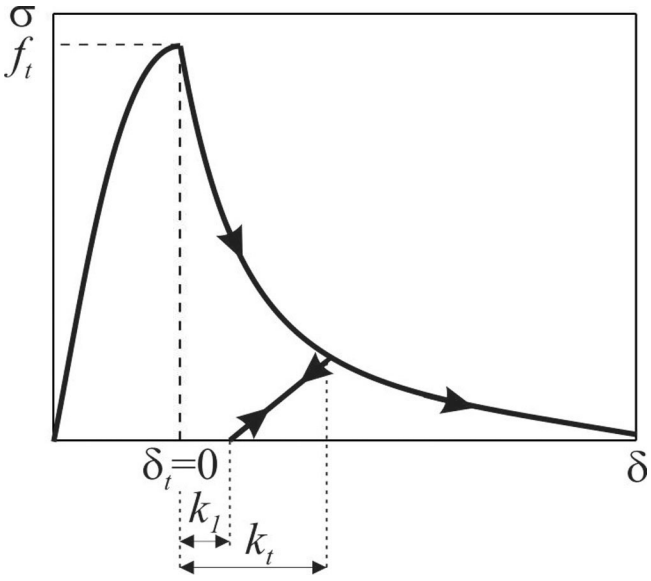

Figure 2. Material model in concrete joint element.
Bild 2. Materialmodell im Betonverbindungselement.

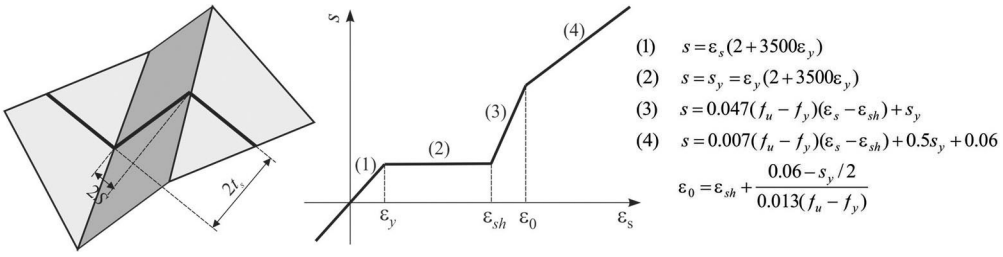

Figure 3. Discrete crack and steel strain-slip relation under monotonic loading.

Bild 3. Diskrete Verhältnisse der Gleit- und Längsverformung bei Rissen und Stahl bei gleichbleibender Belastung.

aration $\delta_t < \delta < \delta_c$, the bonding stress is provided by:

$$\sigma_{cj} = zf_t \tag{3}$$

where z is the heuristic scaling function representing an approximation of the experimental stress-displacement curves taken according to Hordijk [39]:

$$z = \left[1 + (c_1 D_t)^3\right] e^{-c_2 D_t} - D_t\left(1 + c_1^3\right) e^{-c_2} \tag{4}$$

where $c_1 = 3$ and $c_2 = 6.93$, whereas the damage parameter D_t is determined according to the following expression:

$$D_t = \begin{cases} (\delta - \delta_t)/(\delta_c - \delta_t), & \text{if } \delta_t < \delta < \delta_c; \\ 1, & \text{if } \delta > \delta_c \end{cases} \tag{5}$$

The same model for describing the shear stress τ_s and the shear displacement t_s relation is adopted for the concrete behaviour in shear [30].

In this paper, the numerical model in the concrete joint element is extended to capture the main characteristics related to cyclic loading in tension. For this purpose, a material model is adopted, where the ratio of k_1/k_t was obtained experimentally from the uniaxial cyclic tests and is equal to 0.73 [40], *Figure 3*.

One of the most important effects in the modelling of the structures under high impact loading is the increase in the dynamic tensile strength depending on the strain rates. In this paper, a numerical model has been adopted to capture the dynamic behaviour of the concrete subjected to impact loading by introducing dynamic increase factor for the tension that varies with the strain rates. The dynamic increase factor is used according to Comité Euro-International du Béton – International Federation for Structural Concrete Model Code provided by:

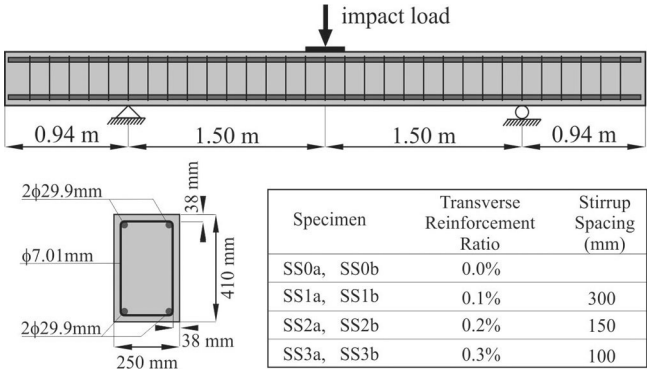

Specimen	Transverse Reinforcement Ratio	Stirrup Spacing (mm)
SS0a, SS0b	0.0%	
SS1a, SS1b	0.1%	300
SS2a, SS2b	0.2%	150
SS3a, SS3b	0.3%	100

Figure 4. Specimen properties [47].

Bild 4. Probeneigenschaften [47].

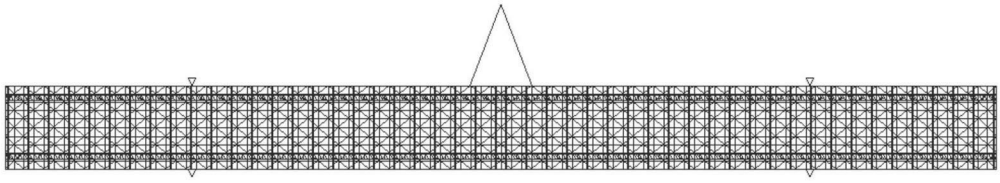

Figure 5. Finite element mesh of the beam.

Bild 5. Finite-Elemente-Netz des Balkens.

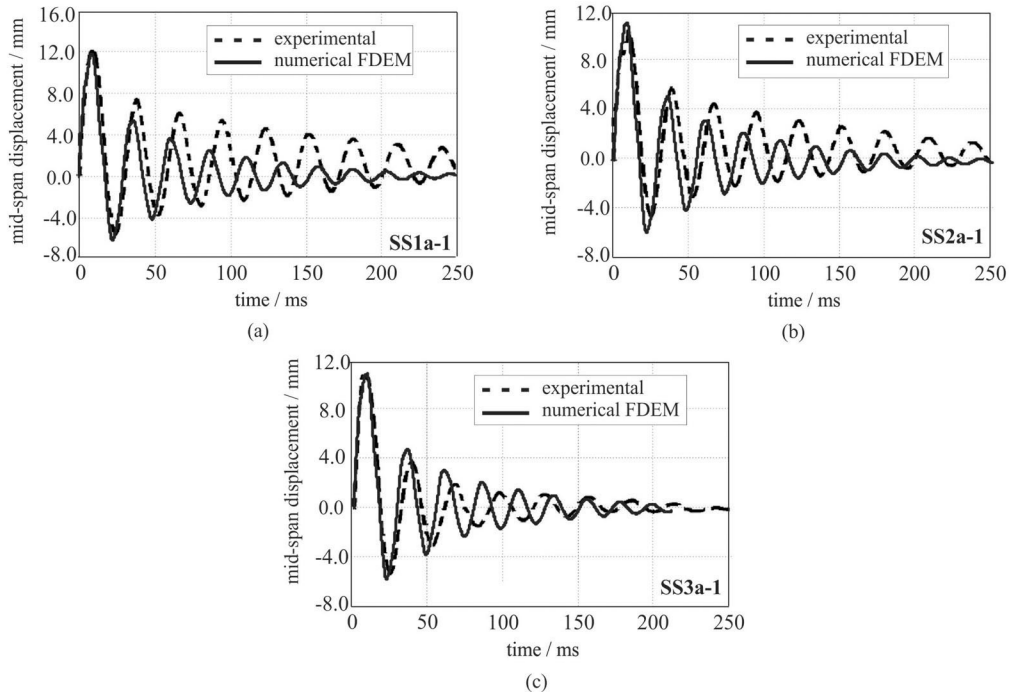

Figure 6. Midspan displacements for the first impact: (a) SS1a, (b) SS2a, (c) SS3a.
Bild 6. Mittelverschiebungen des ersten Aufpralls: (a) SS1a, (b) SS2a, (c) SS3a.

$$\frac{f_{ct}}{f_{cts}} = \left(\frac{\dot{\varepsilon}}{\dot{\varepsilon}_s}\right)^{\delta} \text{ for } \dot{\varepsilon} \le 1s^{-1}$$
$$\frac{f_{ct}}{f_{cts}} = \beta\left(\frac{\dot{\varepsilon}}{\dot{\varepsilon}_s}\right)^{\frac{1}{3}} \text{ for } \dot{\varepsilon} > 1s^{-1} \quad (6)$$

where f_{ct} is the dynamic tensile strength at $\dot{\varepsilon}$, f_{cts} is the static tensile strength at $\dot{\varepsilon}_s$, f_{ct}/f_{cts} is the dynamic increase factor, $\dot{\varepsilon}$ is the strain rate in the range of 10^{-6} to 160 s^{-1} and $\dot{\varepsilon}_s = 10^{-6}s^{-1}$is the static strain rate [41, 42]. The coefficient β in equation (6) is calculated according to the following expressions:

$$\log\beta = 6\delta - 2,\ \delta = \frac{1}{1+\left(8f_c^{'} - f_{c0}^{'}\right)},$$
$$f_c^{'} = f_c + 8 \text{ MPa},\quad f_{c0}^{'} = 10 \text{ MPa} \quad (7)$$

where f_c is the characteristic compressive strength.

2.4 Steel material model in joint element

The material model of steel in the joint element is intended for the simulation of the reinforcing bar between the crack walls. Before the crack opening, the continuity between the reinforcing bar finite elements is ensured through the penalty function method. It is based on the requirement that the ratio of stress in the joint element of the reinforcing bar and the joint element of concrete in the direction of the bar is the same as the ratio of stress in the finite element of the reinforcing bar and the finite element of the concrete.

After the crack opening, the model of the reinforcing bar in the joint element is based on the path-dependent mechanical model for a deformed reinforcing bar at the reinforced concrete interface [43]. The influence of the redistribution of loads along the bar is not directly considered in the finite element as it was taken into account in the bond-slip models, but it is ensured through the local slip and deformation of the bar in the crack according to the experimental curve [44, 45].

An approximation of the experimental crack opening-strain curves is used to describe the behaviour of the reinforcing bar at crack faces. The model

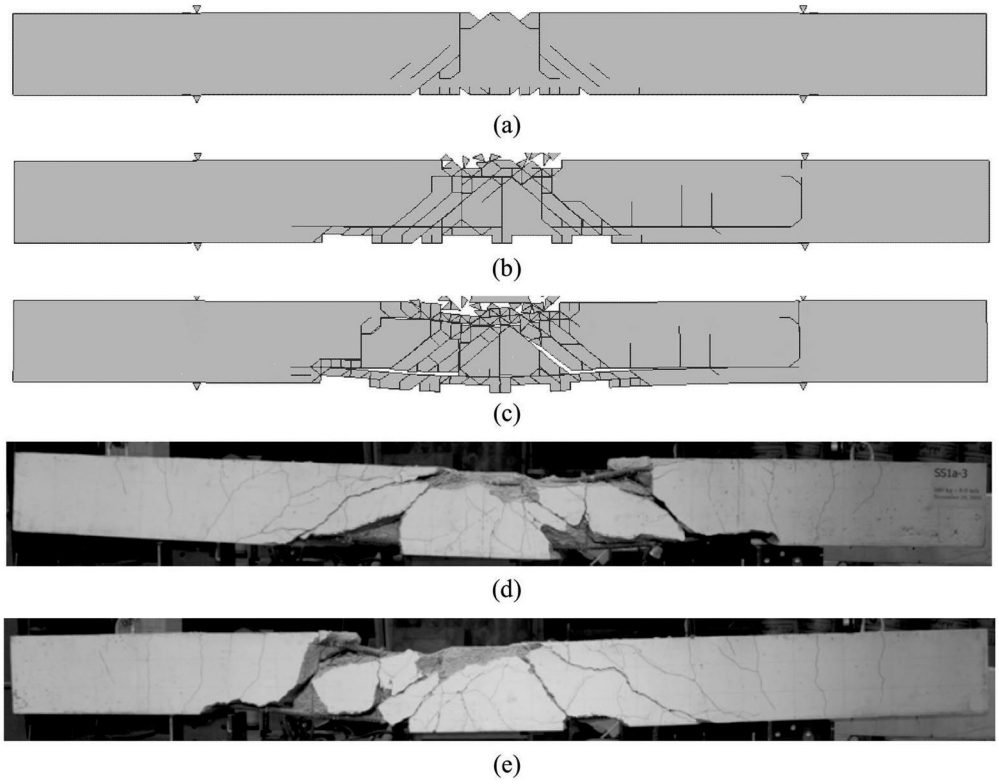

Figure 7. Crack pattern for specimen SS1a: (a) numerical after the first impact, (b) numerical after the second impact, (c) numerical final, (d) experimental final (front side), (e) experimental final (back side).

Bild 7. Rissmuster für die Probe SS1a: (a) numerisch nach dem ersten Aufprall, (b) numerisch nach dem zweiten Aufprall, (c) numerisches Finale, (d) experimentelles Finale (Vorderseite), (e) experimentelles Finale (Rückseite).

takes into account the bond deterioration in the reinforcement near the crack plane and can accurately express the behaviour of the reinforcing bar that undergoes a high plastic deformation under reversed cyclic loading. After the occurrence of the crack, the axial tension force developing in the reinforcing bar is partly transferred to the concrete between the adjacent cracks through bonding between the reinforcing bar and the concrete. Consequently, the local stress along the bar differs from that at the interface. It causes no uniform distribution of strains along the bar which depends on the bar pull out S from the crack interface, Figure 3 [44].

The monotonic slip-strain relations are defined according to the non-dimensional slip s given by:

$$s = \left(\frac{S}{D}\right) K_{fc}, \quad K_{fc} = \left(\frac{f_c}{20}\right)^{2/3} \tag{8}$$

where D is the diameter of the bar, f_c is the concrete compressive strength (MPa) and S is the local slip at any point of the bar obtained by the integration of strain along the bar [43].

In this model, a non-dimensional slip-strain relationship before and after yielding of the steel is used according to the expressions by Soltani and Maekawa, where ε_s is the strain in the reinforcing bar in the crack, ε_y is the yielding strain of the bar, f_u and f_y are the tensile strength and yield stress of steel (MPa), respectively, while ε_{sh} is the strain at the onset of hardening, Figure 3 [43].

After yielding of the reinforcing bar, the normalised steel slip s is expressed as the sum of the slip s_{pl} in the yield region and s_e in the elastic region [43] as:

$$s = s_{pl+}s_e \tag{9}$$

Assuming a linear distribution of strain in the yield region, the normalised steel slip s_{pl} is expressed as:

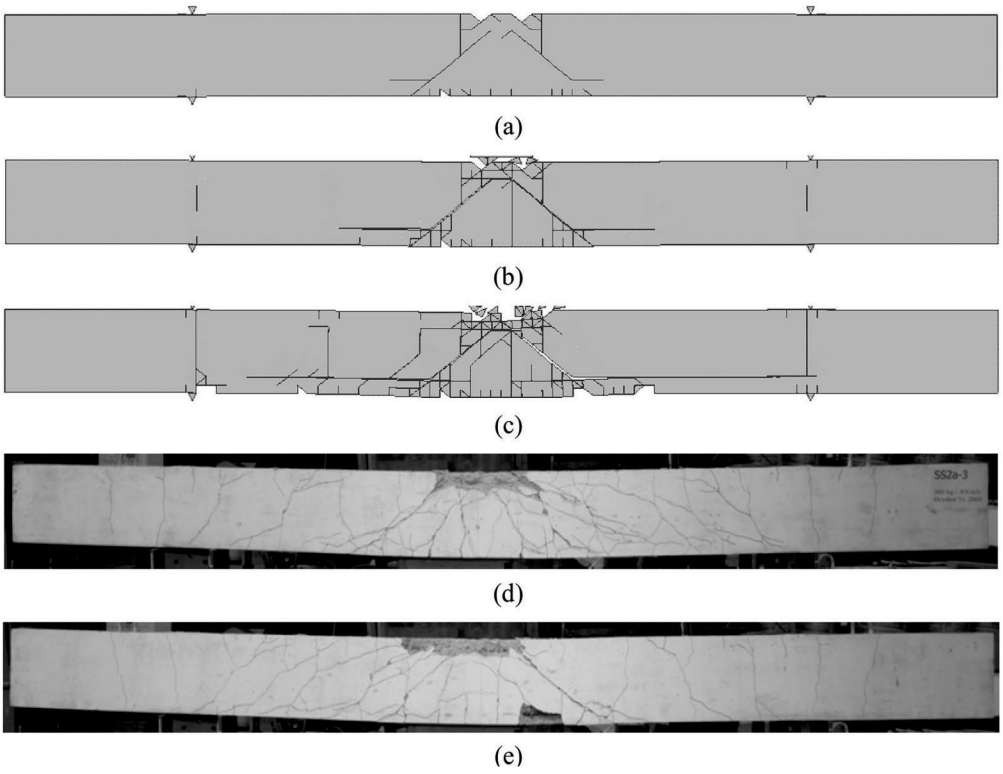

Figure 8. Crack pattern for specimen SS2a: (a) numerical after the first impact, (b) numerical after the second impact, (c) numerical final, (d) experimental final (front side), (e) experimental final (back side).

Bild 8. Rissmuster für die Probe SS2a: (a) numerisch nach dem ersten Aufprall, (b) numerisch nach dem zweiten Aufprall, (c) numerisches Finale, (d) experimentelles Finale (Vorderseite), (e) experimentelles Finale (Rückseite).

$$s_{pl} = \frac{(1+\beta)\varepsilon_s + \varepsilon_{sh} - \beta\varepsilon_{\max}}{\varepsilon_{\max} + \varepsilon_{sh}} \left(s_{\max} - s_y\right) \tag{10}$$

where $\varepsilon_{\max}$ and $s_{\max}$ refer to the steel strain and non-dimensional slip immediately after the change from loading to unloading, β is the factor obtained from the experiments, which approximately equals 1.0. By substituting the equation (10) in (9), the strain in the reinforcing bar at the crack can be obtained from the known non-dimensional slip s.

The calculation of the shear force carried by the bar is based on the experimental curves which describe the curvature of the reinforcing bar in the vicinity of crack faces as a function of deflection of the reinforcing bar at the interface t_s, Figure 3 [45]. The shear force is given by:

$$V_s = E_s I_s \frac{34.9091 t_s}{L_c^3} \tag{11}$$

where E_s is the Young's modulus of the bar, I_s is the moment of inertia of the bar and L_c is the length of the curvature-influencing zone [46].

The influence of the adjacent cracks is approximately taken into account through the reduction factor α which depends on the crack distance l_{cr} [45]. Steel slip s_{cr}, which considers the influence of the adjacent cracks, is expressed as:

$$s_{cr} = \alpha s \tag{12}$$

where s is the non-dimensional slip defined by (8), while the reduction factor α is given by:

$$\alpha = 1 - e^{-(0.065 l_{cr}/D + 0.5)^3} \tag{13}$$

In this model, the position of the crack is defined by the finite element edge, so that l_{cr} is adopted as an input parameter, which is equal to $h/2$, where h is the concrete finite element length.

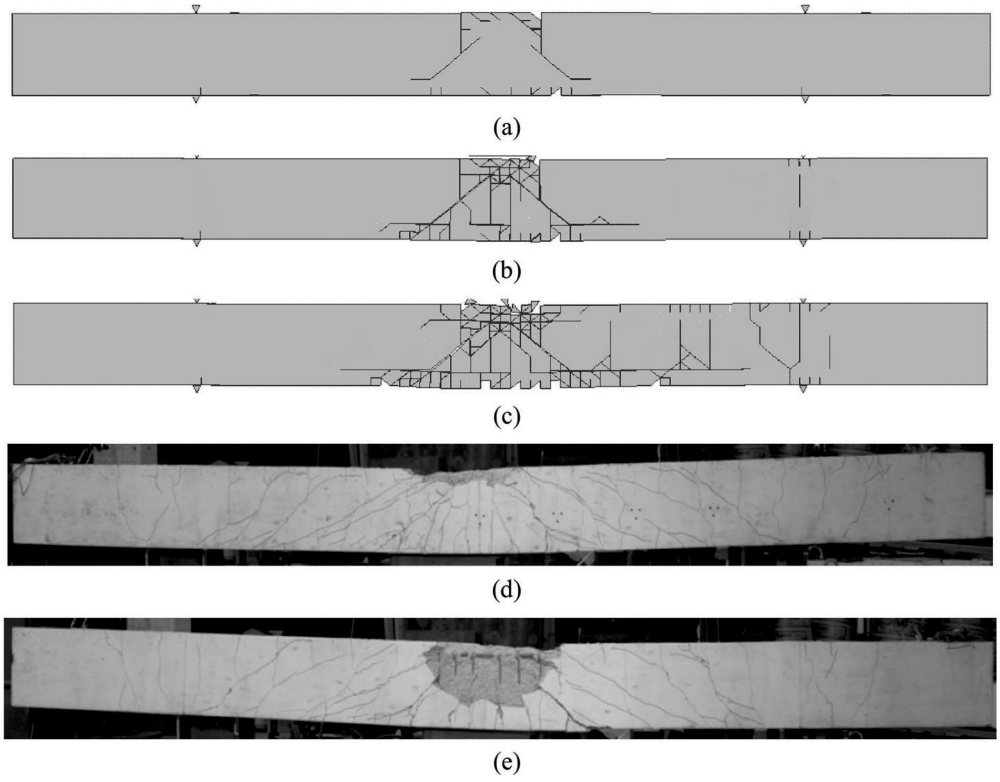

Figure 9. Crack pattern for specimen SS2a: (a) numerical after the first impact, (b) numerical after the second impact, (c) numerical final, (d) experimental final (front side), (e) experimental final (back side).

Bild 9. Rissmuster für die Probe SS2a: (a) numerisch nach dem ersten Aufprall, (b) numerisch nach dem zweiten Aufprall, (c) numerisches Finale, (d) experimentelles Finale (Vorderseite), (e) experimentelles Finale (Rückseite).

3 Numerical example and discussion

An experimental programme conducted at the University of Toronto was selected in order to show the performance of the presented numerical model based on finite-discrete element method in analysing the behaviour of the reinforced concrete structures under impact loading [47]. The experimental programme involved eight simply supported reinforced concrete beams (four pairs) tested under free-falling drop-weights impacting the beams at the midspan. All specimens had geometry with identical longitudinal reinforcement, but with varying shear reinforcement ratios intended to investigate the effects of shear capacity on the impact behaviour, *Figure 4*. Material characteristics are adopted according to available experimental data, *Table 1*. The cross-sectional area of the longitudinal reinforcement was equal to 700 mm^2, whereas the cross-sectional area of the closed stirrups was 38.71 mm^2.

Table 1. Material characteristics of the reinforced concrete beam.

Tabelle 1. Materialeigenschaften des RC-Trägers.

Concrete Specimen	Peak compressive stress (MPa)	Strain at peak compressive stress	Tensile strength (MPa)
SS1a	44.7	$2.36 \cdot 10^{-3}$	5.6
SS2a	47.0	$2.42 \cdot 10^{-3}$	6.2
SS3a	46.7	$2.51 \cdot 10^{-3}$	5.8
Steel Steel bar	Yield stress (MPa)	Yield strain	Ultimate strength (MPa)
longitudinal	464	$2.38 \cdot 10^{-3}$	630
stirrups	605	$3.18 \cdot 10^{-3}$	652

Two different drop-weights were used for the impact testing: a lighter weight of 211 kg and a heavier weight of 600 kg for inducing different lev-

els of damage with each impact. The weights were dropped from a clear height of 3.26 m above the specimen, resulting in the calculated impact velocity of 8.0 m/s. All specimens, with the exception of SS0b, were subjected to multiple impacts. With the a-series specimens, the beams were tested once with the lighter drop-weight followed by two tests with the heavier one. For b-series specimens, the order was reversed; they were tested twice with the heavy drop-weight, and then one last time with the lighter drop-weight. The beams analysed within this paper, i. e. specimens SS1a, SS2a and SS3a, were first tested once with the lighter drop-weight, followed by two tests with the heavier one.

In the numerical analyses, a damping coefficient $\bar{\mu}$ was equal to 23.2×10^6 (N/m^2/s) in order to obtain better correlation with the experimental test data. In this model, the energy dissipation during the impact was not modelled at the contact between the drop-weight and the beam. It was enforced in the finite elements of the block and the base according to equation (4). When the drop-weight and beam are in contact, the rate of the deformation causes energy dissipation due to the occurrence of the damping forces in the finite elements of the beam.

The discretisation of the beams was performed by using 1960 triangular finite elements, *Figure 5*.

The comparison of the experimental and numerical midspan displacement in time for the first impact shows good agreement, *Figure 6*. Peak displacements were captured with considerable accuracy. Some discrepancies, however, were observed in the post-peak vibrations. For all tests, the analyses predict a somewhat shorter period of vibration compared to the test measurements. Damping for the specimens SS1a and SS2a was overestimated, which resulted in smaller calculated displacements amplitudes.

The crack patterns after the first, second and third impact obtained by the numerical analysis and the final crack patterns and failure modes obtained experimentally are presented, *Figures 7–9* [47]. It is discernible that for all tests the number of cracks increases with the increased number of impacts. Also the final crack profiles were predicted rather well.

All specimens developed severe diagonal cracks originating at the impact point and propagating downward with an angle of approximately 45° and forming shear plugs. In addition, several diagonal cracks parallel to the major shear-plug cracks also developed, along with some vertical flexural cracks at the midspan and at the supports. It is evident that the diagonal cracks in the beam whose inclination increases towards the supports were predicted correctly. Shear plug formations were also correctly represented in all specimens.

The results of the research performed within this paper show that the numerical analysis using the presented model can efficiently and realistically simulate the impact behavior of the reinforced concrete beams. The peak displacement, crack pattern, damage level and failure modes as obtained from the analysis are in close agreement with their experimentally observed counterparts.

4 Conclusions

This paper presents the performance of numerical model based on the combined finite-discrete element method for the prediction of the structural response of the reinforced concrete beams under impact loads. Based on the comparison of the experimental beam impact test results with the numerical results obtained by the presented model based on combined finite-discrete element method, the following conclusions can be drawn:

- The proposed numerical model performed well in predicting peak displacements and damage levels of the reinforced concrete beams under impact loads.
- Post-peak vibration characteristics, compared between the test results and the presented numerical model showed some minor discrepancies. These discrepancies were mostly attributed to the deficiencies regarding the modelling of the hysteresis behaviour of concrete and steel under high strain rate conditions.
- The proposed numerical model was also successful in predicting the crack pattern of the damaged specimens for the third impact tests on the same specimens. This indicates that the presented numerical model is capable of accurately modelling the reduced stiffness of the reinforced concrete structure after it suffers considerable levels of damage.
- The contact interaction algorithm based on the potential contact forces completely eliminated the need for an impact force history. The only required parameters for the impact analysis with the

proposed numerical model were the drop-weight mass, its impact velocity and the damping coefficient which considers the energy dissipation during impact.
- Finally, the presented results demonstrated the ability of the presented numerical model for the realistic simulation of the behaviour of reinforced concrete beams under impact loading.

Acknowledgements

This paper has been entirely supported by the Croatian Science Foundation under the project Development of numerical models for reinforced-concrete and stone masonry structures under seismic loading based on discrete cracks (IP-2014-09-2319).

5 References

[1] A. Haldar, F.J. Miller, *Nucl. Eng. Des.* **1982**, *71*, 79.
[2] G. Hughes, *Nucl. Eng. Des.* **1984**, *77*, 23.
[3] J. Feng, W.B. Li, G.W. Pan, X.M. Wang, *Acta Mech.* **2017**, *228*, 401.
[4] P.H. Bischoff, S.H. Perry, J. Eibl, *Int. J. Impact. Eng.* **1990**, *9*, 317.
[5] T. Krauthammer, S. Shahriar, H.M. Shanaa, *J. Struct. Eng.* **1990**, *116*, 1061.
[6] A. Nobili, E. Radi, L. Lanzoni, *Acta Mech.* **2016**, *227*, 159.
[7] S.M. Kulkarni, S.P. Shah, *ACI Struct. J.* **1998**, *95*, 705.
[8] N. Kishi, H. Mikami, K.G. Matsuoka, T. Ando, *Int. J. Impact. Eng.* **2002**, *27*, 955.
[9] M. Zineddin, T. Krauthammer, *Int. J. Impact. Eng.* **2007**, *34*, 1517.
[10] D.M. Cotsovos, *Int. J. Impact. Eng.* **2010**, *37*, 907.
[11] S.D. Adhikary, B. Li, K. Fujikake, *Int. J. Impact. Eng.* **2012**, *47*, 24.
[12] D.K. Thai, S.E. Kim, *Eng. Failure Anal.* **2014**, *45*, 252.
[13] T. Zhan, Z. Wang, J. Ning, *Eng. Failure Anal.* **2015**, *56*, 233.
[14] B. Rebora, T. Zimmerman, J.P. Wolf, *Nucl. Eng. Des.* **1976**, *37*, 269.
[15] Y.M. Gupta, L. Seaman, *Nucl. Eng. Des.* **1978**, *45*(2), 507.
[16] V. Adamik, P. Matejovic, *Nucl. Eng. Des.* **1989**, *113*, 111.
[17] V. Travaš, J. Ožbolt, I. Kožar, *Int. J. Fract.* **2009**, *160*, 31.
[18] J. Ožbolt, A. Sharma, *Int. J. Impact. Eng.* **2011**, *38*, 940.
[19] N. Kishi, A.Q. Bhatti, *Int. J. Impact. Eng.* **2010**, *37*, 103.
[20] K. Shirai, C. Ito, H. Onuma, *Nucl. Eng. Des.* **1994**, *150*, 483.
[21] H. Jiang, X. Wang, S. He, *Mater. Des.* **2012**, *39*, 111.
[22] K. Thoma, D. Vinckier, *Nucl. Eng. Des.* **1994**, *150*, 441.
[23] L. Agardh, L. Laine, *Int. J. Impact. Eng.* **1999**, *22*, 911.
[24] Y. Sawamoto, H. Tsubota, Y. Kasai, N. Koshika, H. Morikawa, *Nucl. Eng. Des.* **1998**, *179*, 157.
[25] S.A. Magnier, F.V. Donzé, *Mec. Cohes.-Frict. Mater.* **1998**, *3*, 257.
[26] W. Shiu, F.V. Donzé, L. Daudeville, *Int. J. Comput. Appl. Tech.* **2009**, *34*, 33.
[27] R.P. Nair, C.L. Rao, *Int. J. Comput. Methods Eng. Sci. Mech.* **2014**, *15*, 9.
[28] A. Munjiza, *The Combined Finite-Discrete Element Method*, John Wiley & Sons, London, **2004**.
[29] T. Bangash, A. Munjiza, *Comput. Mech.* **2003**, *30*, 366.
[30] N. Živaljić, *Ph.D. Thesis*, University of Split, Croatia, **2012**.
[31] N. Živaljić, H. Smoljanović, Ž. Nikolić, *Eng. Comput.* **2013**, *30*, 982.
[32] I. Uzelac Glavinić, H. Smoljanović, M. Galić, A. Munjiza, A. Mihanović, *Materialwiss. Werkstofftech.* **2018**, *49*, 635.
[33] H. Smoljanović, I. Uzelac Glavinić, B. Trogrlic, N. Zivaljic, A. Munjiza, *Materialwiss. Werkstofftech.* **2018**, *49*, 651.
[34] A. Munjiza, K.R.F. Andrews, J.K. White, *Int. J. Numer. Meth. Eng.* **1998**, *43*, 131.
[35] A. Munjiza, K.R.F. Andrews, J.K. White, *Int. J. Numer. Meth. Eng.* **2000**, *49*, 1337.
[36] S. Saatci, F.V. Vecchio, *ACI Struct. J.* **2009**, *106*, 78.

[37] J. Xiang, A. Munjiza, J.P. Latham, R. Guises, *Eng. Comput.* **2009**, *26*, 673.
[38] A. Munjiza, K.R.F. Andrews, J.K. White, *Int. J. Numer. Meth. Eng.* **1999**, *44*, 41.
[39] D.A. Hordijk, *Heron* **1992**, *37*, 3.
[40] H.V. Reinhardt, *Heron* **1984**, *29*, 3.
[41] *CEB-FIB Model Code 1990, Design Code*, Lausanne, Switzerland, Thomas Telford, **1993**, pp. 437.
[42] D.L. Hevroni, E. Kochavi, B. Kofman, S. Gruntman, O. Sadot, *Int. J. Imp. Eng.* **2018**, *114*, 93.
[43] M. Soltani, K. Maekawa, *Eng. Struct.* **2008**, *30*, 1079.
[44] A. Ibrahimbegovic, A. Boulkertous, L. Davenne, D. Brancherie, *Int. J. Numer. Meth. Eng.* **2010**, *83*, 452.
[45] K. Maekawa, A. Pimanmas, H. Okamura, *Nonlinear Mechanics of Reinforced Concrete*, Spon Press, London, **2003**.
[46] J. Qureshi, K. Maekawa, *Proc. of JCI*, **1993**, *15*, 1249.
[47] S. Saatci, *Ph.D. Thesis*, University of Toronto, Canada, **2007**.

Received in final form: December 14th 2018

